LAWRENCE
LIVERMORE
NATIONAL
LABORATORY

LLNL-JRNL-414426

Local Scrape-Off Layer Control Using Biased electrodes in NSTX

S. J. Zweben, R. J. Maqueda, A. L. Roquemore, C. E. Bush, R. Kaita, R. J. Marsala, Y. Raitses, R. H. Cohen, D. D. Ryutov

July 2, 2009

Plasma Physics and Controlled Fusion

Disclaimer

Local scrape-off layer control using biased electrodes in NSTX

S.J. Zweben, R.J. Maqueda[a], A.L. Roquemore, C.E. Bush[b], R. Kaita, R.J. Marsala, Y. Raitses, R.H. Cohen[c], D.D. Ryutov[c]

Princeton Plasma Physics Laboratory, Princeton NJ USA

(a) Nova Photonics, Princeton NJ USA

(b) Oak Ridge National Laboratory, Oak Ridge TN USA

(c) Lawrence Livermore National Laboratory, Livermore, CA USA

Abstract

An experiment was designed to test the theory that biased electrodes can affect the local scrape-off layer (SOL) width by creating a strong radial ExB drift [Cohen, R.H. and Ryutov, D.D, Nucl. Fusion 37, 621 (1997)]. These electrodes were located near the outer midplane in the SOL of the National Spherical Torus Experiment (NSTX). The electrodes were biased at up to ±100 Volts, and the radial profile of the plasma between them was measured by an array of Langmuir probes. The biasing caused large changes in the local SOL profiles at least qualitatively consistent with this theory.

1. Introduction

It is well known that the highly localized power and particle flux to the divertor plates of a tokamak creates difficult problems for the operation of ITER [1,2]. This localization is due to the large ratio of parallel to perpendicular transport in the scrape-off layer (SOL), which causes the radial width of the SOL to be typically ~1 cm at the divertor plates. This radial transport depends on the SOL turbulence and so can not yet be predicted from first principles, so empirical scalings for the SOL width have been used for many year to extrapolate to future devices, e.g. [3,4].

Obviously it would be desirable to develop methods to externally control the SOL width of a tokamak. One proposal has been to use asymmetric electrical biasing to create local convective cells to control the local radial SOL flow [5-7]. Such biasing could create a $v_{rad}=E_{pol}xB$, flow larger than the radial flow speed of the turbulence, leading to a displacement or a broadening of the SOL at the divertor plate. Note that this type of biasing creates an *asymmetric poloidal* electric field, in contrast to previous experiments which created an *symmetric radial* electric field [8,9].

The present experiment was designed to test the principles of this theory using a set of biased electrodes in the SOL near the outer midplane of NSTX. After a review of previous experiments (Sec. 2), we describe the experimental set-up in NSTX (Sec. 3), the effects of biasing on the local SOL profiles, (Sec. 4), other experimental results (Sec. 5), a comparison with theoretical models (Sec. 6), and a discussion and summary (Sec. 7).

2. Previous experiments

There have been several previous experiments to control the SOL plasma using externally applied ExB drifts. A radial electric field was used to modify plasma flow in the poloidal divertor of the Wisconsin Octopole [10], and various divertor plate biasing methods were tried in the TdV tokamak [11], Control of particle exhaust was attempted with a biased toroidal divertor ring on DIII-D [12], and with a biased pumped divertor in TEXTOR [13]. Local radial electric fields were proposed to control the plasma interaction with RF antennas [14,15]. There also is an extensive literature on electrode biasing to create a radial electric field to control edge transport [8,9].

Several tokamak experiments have been done to understand the downstream effects (along B) of probe biasing in the SOL. A positive DC plate bias in DITE changed the floating potential in a probe ~2.5 mm away along B [16]. A positive DC and 30 kHz oscillating bias were TEXT were detected ~12 m away along B [17], and a 60 KHz probe bias in W7-AS was observed at a distance up to ~12 m away along B [18]. Changes in the local floating potential were observed near a biased probe in Alcator C-Mod [19]. The operation of Langmuir probes is a tokamak is also closely related to questions about the downstream effects of biasing [20,21].

A few previous experiments have attempted to create convective cells and radial flows in the SOL using asymmetric biasing. In JFT-2M [22] an electrical bias of +120 volts was applied to an inner wall divertor plate and a poloidal electric field of ~10 V/cm was measured at the midplane where the

magnetic field lines connected to the biased plate. In MAST [23] an electrical bias of +80 to +120 volts was applied to 6 toroidally separated divertor 'ribs', and a movement of the D_α emission was seen at these ribs in the expected ExB drift direction. In CASTOR [24] an electrode was biased +100 to +200 volts in the SOL, a poloidal electric field of up to 5 kV/m was created on flux surfaces connected to the electrode, and a strong poloidal modulation of the radial particle flux was measured.

Preliminary reports on the NSTX electrode biasing experiments were presented previously describing the diagnostics and electrode design [25] and the results from an initial set of experiments [26]. The present paper contains additional experimental results and more detailed analysis.

3. Experimental Set-up on NSTX

The general experimental set-up on NSTX is illustrated in Fig. 1. The electrodes are 3 cm x 3 cm square stainless steel plates flush-mounted into a boron nitride holder located ~25º below the outer limiter. The electrodes are aligned approximately normal to the total plasma magnetic field in this region, and the leading edge of the mounting plate is ~ 1 cm radially behind the leading edge of the RF antenna limiter just behind the electrodes. Thus the electrodes interact with the SOL plasma in only one direction along B, and the field lines in this direction extended ~1 to ~8 meters along B before hitting any other object in the SOL (depending on the details of the plasma equilibrium). The electrodes were at a fixed location for these experiments.

A scale drawing of the NSTX electrodes is shown in Fig. 2. The four electrodes were separated in the local poloidal direction with a gap of 1 cm between them. The leading edges of the electrodes were 0.3 cm behind the leading edge of the boron nitride holder. Each electrode could be independently biased up to ±100 volts with respect to the local vessel wall and could draw up to 30 amps per electrode for positive bias or 10 amps per electrode for negative bias. The electrode power supplies could be turned on and off anytime during the discharge, and were modulated at 50 Hz for clearer comparison of electrode on and off states. Each of the four electrode voltage and current signals were digitized at 20 kHz. Most of the data in this paper was taken with biasing only on electrodes #2 and #3.

The local effects of the electrode biasing were measured with a set of flush-mounted stainless steel Langmuir probes of 0.3 cm diameter installed in the electrode holder, as also shown in Fig. 2. Five of these probes could be DC biased up to ±50 volts with respect to the local vessel wall, or swept in voltage or 'floated'. Most of the results in this paper were taken using the four probes in the radial array P3a-P3d. The current and voltage signals from the probes were digitized at 200 kHz. Both the electrodes and probes had ~1 mm gaps at and below their edges to prevent arcing, and no arc tracks between electrodes and/or probes were seen after the run.

The other main diagnostic used in this experiment was the gas puff imaging (GPI) system, also shown in Fig. 1. The GPI gas puff manifold was located ~1 meter downstream along B from the biased electrodes, and was used to measure the effects of electrode biasing on the SOL plasma at this location, as described in Sec. 5(b). Further information concerning the

electrodes and probe hardware for this experiment are described elsewhere [25]. A preliminary report on the NSTX biasing experiments can be found in [26], and information on the GPI diagnostic on NSTX can be found in [27].

4. Effects of biasing on the local radial profiles

This section describes effects of electrode biasing on the Langmuir probes adjacent to the biased electrodes, especially those in the radial array of Fig. 2. The results of Secs. 4(a)-(c) are for Ohmic lower single null diverted plasmas, but NBI and RF heated plasmas are qualitatively similar, as described in Sec. 4(d). Results from the GPI diagnostic and other 'downstream' effects are discussed in Sec. 5.

4.1 Time dependences

The typical time dependence of the electrode voltages and currents in this experiment is shown in Fig. 3. As shown at the left, the bias voltages were kept constant during a shot but modulated in phase at 50 Hz to better compare the "bias on" (with respect to the vessel ground) vs. "bias off" (i.e. floating) states. The electrode currents also varied with the width of the outer "gap" between the separatrix and the outer midplane limiter and with the line-averaged density. On a faster timescale as shown at the right, the electrode currents responded within 1 msec to changes in the electrode voltages, as did the signals from the probes. The large fast fluctuations on the electrode and probe currents are due to SOL turbulence.

b) Electrode and probe (I,V) characteristics

Fig. 4(a) shows a typical (I,V) characteristic for the electrodes in the range -90 V to + 90 V with respect to the nearby vessel ground, i.e. "normal" biasing. The positive values were from electrode E3 and the negative values from electrode E2 for the same shots (#129500-129505), and both were time averaged over 0.2-0.3 sec. The ratio of electron to ion currents was ~8 at ±90 Volts, and the floating potential of the electrodes was ~ 0 Volts. Also shown in Fig. 4(a) is a "floating" current point obtained on a similar discharges (#129402,3) when electrode E3 was biased by +90 V with respect to E2. The current in this "double-probe" configuration was about the same as the ion saturation current in the normal configuration, as expected.

Fig. 4(b) shows a typical (I,V) characteristic of one of the probes, in this case the probe #3a between electrodes #2 and #3. For this shot (#129506) the probe voltage was swept between ± 50 V at 200 Hz, and curves for the electrodes "bias on" (E2 = -90 V, E3 = +90 V) and "bias off" are shown separately. These curves are each averaged over ~14 voltage sweeps over 0.2-0.34 sec, and the results are binned in 1 volt increments. The electron current does not show a clear saturation, and the ratio of the probe electron current +45 V to the probe ion current at -45 V was ~15-20. There is also a slight (~ 5 volt) increase in the floating potential for the "bias on" state compared to the "bias off" state. The ratio of the ion current in the electrode E2 at -90 Volts to the ion current in the nearby probe (P3a) at -50 Volts is ~ (1 A/0.01 A) ~ 100, which is near to the ratio of the electrode area to the probe area (~ 9 cm^2/0.7 cm^2 ~ 100), as expected.

The electron temperatures and density profiles inferred from similar probe voltage sweeps are shown in Fig. 5(a). In these plots the horizontal scale is the radial position of the probes in the radial array as measured with respect the first probe (#P3a), which is centered between electrode E2 and E3 (see Fig. 2). The electron temperatures were averaged over 0.2-0.34 sec for two similar shots (#129506, 129510), and was T_e~5-10 eV, with perhaps a slight increase with the ±90 V biasing on. The radial profiles of the electron density inferred from these same probe sweeps are shown in Fig. 4(b). The red curves are for the bias "bias on" state, while the blue curves are for the bias "off" state. The solid lines are the ion saturation ("isat") currents (-47 V to -40 V), from which the electron density was inferred using $I(isat) = 0.5\ n\ e\ c_s$. The density ranges from ~10^{12} cm^{-3} for the probe nearest the plasmas to ~10^{11} cm^{-3} for the probe farthest from the plasma. The dashed lines are the electron saturation ("esat") current profiles measured from the same sweeps (+40 V to +45 V), normalized to the corresponding "isat" points at r=0. The "esat" profiles are similar to the "isat" profiles, and respond similarly to the biasing.

Most of the radial profile measurements in this paper were made using the electron saturation current, i.e. with the probes at +50 V, since this allowed the system to be switched from DC biasing to swept mode without any hardware changes. These profiles are used to measure the relative change in plasma flux or plasma density due to electrode biasing. The similarity of the electron and ion profiles shown in Fig. 5 indicate that these results are equivalent to more commonly used ion saturation current profiles.

c) Variation with electrode bias voltage

The effect varying the electrode bias voltage on the radial profiles of electron saturation current in the radial probe array is shown in Fig. 6. This figure demonstrates the basic result from this experiment; namely, large and systematic changes increase in the SOL width due to electrode biasing.

Figure 6(a) shows that the effects of biasing start at about ±10 Volts and begin to saturate above about ±50 Volts. The plasmas used for Fig. 6(a) are the same as used for Fig. 3-5, i.e. Ohmic LSN plasmas (#129500-129505). As for Figs. 3-5, there was a negative voltage on electrode E2 and an equal positive voltage on electrode E3, with the voltages modulated in time as in Fig. 3 and varied in magnitude from shot-to-shot. The sign of the poloidal electric field between electrodes E2 and E3 was such that the resulting ExB drift direction was radially outward. Electrodes E1 and E4 were grounded. The curves shown in Fig. 6(a) are the averages over 0.2-0.34 sec, i.e. over ~ 7 "bias on" and 7 "bias off" periods for each shot. There was very little shot-to-shot variation in the profiles during the biasing 'bias off' times, as expected.

Figure 6(b) shows a larger set of data on the effects of the electrode bias voltage (20 Ohmic shots within #129473-505). The vertical axis is the ratio of electron saturation currents for the third radial probe (r=2.5 cm) during each individual "bias on" time period, divided by that in the subsequent "bias off" time period. The red circled points are the same as those in Fig. 6(a), the purple triangles are shots with the same plasma current (800 kA) but ~50% lower line averaged density, and the blue solid dots are

at 600 kA and ~50% higher density. The signal levels in the r=2.5 cm probe increased with biasing by roughly x5 at up to ±90 Volts, with a fairly large scatter in the results but without much variation with plasma current or density.

d) Variation with type of heating

Results for plasmas with other types of heating are shown in Figure 7, where solid lines are for "bias on" and dashed lines are for "bias off". The SOL profiles become broader with electrode biasing in all cases.

Figure 7(a) shows three different cases: ±90 V bias for OH discharges (7 shots, 32 on/off cycles), ±90 V for 2-4 MW NBI discharges (4 shots, 32 cycles), and ±50 V for 1-2 MW RF cases (4 shots, 19 cycles). As for Figs. 3-6, the ExB drift direction was outward between electrodes E2 and E3. For the OH and RF cases electrodes E1 and E4 were grounded, while for the NBI cases electrode E1 was grounded and E4 was biased the same as E2. For the NBI plasmas the L-mode and H-mode behavior was similar, as described previously [26]. For all cases I=600-800 MA and B=4.5-5.5 kG.

Figure 7(b) shows that the ratio of the electron saturation currents with "bias on" to "bias off" is for the outermost probes is ~ 5-10. For OH plasmas the innermost probe current changes very little or decreases with biasing (P3a, just between the electrodes), while for RF and NBI plasmas this probe current increases significantly. For OH plasmas the radial profile during biasing is almost flat, while for RF and NBI plasmas the profiles fall with radius.

Figure 7(c) shows the floating potential profiles for these different types of plasmas. For OH and NBI the floating potentials are near zero without biasing and become more positive with biasing, especially in the probes nearest the radius of the electrode location (i.e. r $\leq$ 1.25 cm). For the RF case the floating potential is very negative without biasing due to the RF itself, but also become more positive with biasing. These changes in floating potential are generally $\leq$10 V and so are much less than the bias voltages of ±90 V for the OH and NBI cases and ±50 V for the RF case.

e) Variation with electrode polarity and grounding

For all results so far the electrode E2 was biased positive and E3 was biased negative, which create an outward ExB drift at the radial probe array. This section describes what happened when the polarity of these electrodes was varied.

Figure 8(a) shows the electron saturation current profiles when the electrode polarity was reversed, i.e. E2 positive and E3 negative (at the same voltage), so that the ExB drift was radially *inward* at the probe array. This data was averaged over 5 NBI shots similar to those in Fig. 7 (#130092-96), with 2 MW of NBI at I=800 kA and B=5.5 kG, and with a total of 32 "bias on" and 32 "bias off" cycles. The E2, E3 electrode voltages were in the range ±50 V to ±90 V, and electrodes E1 and E4 were grounded. In this case the innermost probe current decreased by about x10 with biasing, while the outermost probe currents increased by about 10 with biasing.

Figure 8(b) shows the electron saturation current profiles when the electrode polarities of E2 and E3 were *both positive* (at the same voltage). This data was averaged over 6 NBI shots similar to those in Fig. 8(a) (#130064-71), with 3 MW of NBI at I=900 kA and B=4.5 kG, and with a total of 30 "bias on" and 30 "bias off" cycles. The E2 and E3 electrode voltages were in the range ±50 V to ±70 V, and electrodes E1 and E4 were grounded. The results with this biasing were similar to the reversed polarity case of Fig. 8(a), e.g. the current in the innermost probes decreased by about x10 times with biasing.

Figure 9 shows the electron saturation current profiles when only *one* electrode was biased. For figure 9(a) electrode E3 was +50 V and E2 was grounded (along with E1 and E4), while for Fig. 9(b) electrode E2 was -50 V and E3 was grounded (along with E1 and E4). This data was averaged over 2 OH shots for each case (127165,166 or 127184,185), with at I=600 kA and B=5 kG, and with a total of 6 "bias on" and 6 "bias off" cycles. The profiles with only one electrode at +50 V were similar to those at ±50 V biasing in this sequence of shots (not shown), while the profiles for -50 V only showed almost no change with biasing. Thus almost all the effects of biasing were due to the positive electrode, and almost no effects were due to the negative electrode.

Figure 10 shows the electron saturation current profiles when electrode E3 was biased +90 V with respect to E2, i.e. when the two electrodes E2 and E3 were floating with respect to ground (as in a double probe), while electrodes E1 and E4 were grounded. This configuration was of interest because the current (and power) drawn by the electrodes was

significantly lower than when the electrodes were biased with respect to the wall, as was the case in all previous figures. This data was averaged over 4 OH shots (#129402-407), with I=800 kA and B=4.5 kG, and with a total of 32 "bias on" and 32 "bias off". These profiles show some broadening of the profiles with biasing, but less than with ±90 V biasing of the electrodes with respect to ground, as in Fig. 6(a).

5. Effects of biasing on turbulence and other results

Section 4 described the effects of electrode biasing on the local radial profiles as measured by the probes between the biased electrodes. This section describes other types of measurements made during these same biasing experiments.

a) Effects on the local turbulence

Figures 11-12 show the effects of electrode biasing on the turbulence measured by the radial probe array between electrode #2 and #3 (# P3a-P3d). For this data the bias level was ±70 or ±90 Volts with respect to vessel ground in the 'normal' direction for Ohmic plasmas, i.e. with the radial ExB drift outward. The fluctuations were measured in the electron saturation current signals for 8 Ohmic plasmas in the data set of Fig. 6, including a total of 48 "bias on" / "bias off" cycles.

The relative fluctuation levels without biasing are in the range ~30% to 90% (rms/mean), as usual for SOL turbulence in NSTX and other tokamaks, as shown in Fig. 11(a). These relative fluctuation levels show a systematic decrease by up to x2 in the radial regions where the local density was increased with biasing, as in Figs. 5-6. The autocorrelation times shown in Fig. 11(b) are in the range ~20 to 40 μs, also similar to previous NSTX SOL measurements. The autocorrelation times are perhaps slightly, but not significantly, decreased by the biasing.

The zero-time-delay cross-correlation coefficients between the probe at r=0 cm and the other probes in the radial array is shown in Fig. 12(a). The radial correlation lengths is ~4 cm (FWHM), as in previous NSTX SOL measurements. The biasing has no significant effect on the radial cross-correlation coefficients. The radial turbulence speed also was determined from the delay time of the peak in the cross-correlation between the probe at r=0 cm and the other probes, as shown Fig. 12(b). Without biasing the turbulence propagated dominantly in the radially outward direction, as usual for the NSTX SOL [28]. There was a small increase in the outward radial propagation speed with biasing from ~1.4 km/sec to ~2.3 km/sec, but this was only slightly outside the standard deviations from these measurements. No statistically significant differences in the radial turbulence speed with vs. without biasing was measured in cases with NBI or with reversed polarity, but the number of bias cycles was lower and the statistical variations larger than for Fig. 12(b).

b) Gas puff imaging results

The gas puff imaging (GPI) diagnostic is shown in Fig. 1 and was described briefly in Sec. 3. The radial and poloidal profiles of the D_α emission from the GPI gas cloud were measured ~1 meter downstream along B from the biased electrodes. The average D_α emission responds to changes in the average density and/or electron temperature, and the fluctuations in the D_α respond to changes in the local turbulence.

The GPI images were spatially aligned with the electron saturation current signals from the Langmuir probes of Fig. 2 by cross-correlating their turbulent fluctuations. The maximum cross-correlation coefficient between the GPI and the probe #3a was ~0.75-0.78, so these two diagnostics are responding to the same turbulent 'filaments', which are well known to have a large correlation length along B. A 2-D image of the cross-correlation coefficients showing good alignment of all 5 probes was in Ref. [25].

Using this alignment, the radial profile of the average D_α light along the radius of the probe radial array is shown in Fig. 13(a) for one shot (#127054), which was one of the NBI shots of Fig. 7. The radial scale goes from -6 cm to +2 cm with respect to the r=0 cm probe location (outside of which the D_α signal level was too small to be reliably measured). The radial profiles during 4 bias "on" cycles were negligibly different from the adjacent bias "off" cycles (as were the poloidal profiles). Thus there was no measurable effect on the density and/or temperature profiles at the GPI location due to the electrode biasing.

The GPI signals along this same radial axis for the same shot were used to calculate the delay times of the peak of the cross-correlation function vs. radius for the turbulence propagation, just as for Fig. 12(b). The resulting delay times are shown in Fig. 13(b) for the same data set as for Fig. 13(a). There was a small increase in the outward radial propagation speed with biasing from ~0.9 km/sec to ~1.3 km/sec, but this was only slightly outside the statistical uncertainty in these measurements. There were also small changes over this same radial range in the autocorrelation times (26 μs with "bias on" vs. 17 μs "bias off"), the radial correlation lengths (3.8 cm FWHM with "bias on" vs. 2.8 cm FWHM "bias off"), and the poloidal correlation length (3.6 cm FWHM with "bias on" vs. 5.0 cm FWHM "bias off"). However, these changes were also not far outside the statistical uncertainty in these measurements.

A movie of the GPI data showing the turbulence structure and motion with and without biasing for this shot can be seen at: [http://www.pppl.gov/~rmaqueda/other/movie_127054.avi]. It seems as if the blobs move outward between the electrodes more often when the bias is on, but this behavior is not very clear. Further analysis of this data is beyond the scope of the present paper.

c) Direct imaging of the electrodes

The visible light from the region of the biased electrodes was imaged by two different fast cameras. Using a camera having the view of Fig. 1, the electrodes were normally the same brightness as the surrounding regions,

and no extra light was observed with electrode biasing. When the outer gap was very small, or the NBI power was large, there was additional light from the edge of the electrode holder (and the nearby RF antenna), but little or no additional light from the electrodes during biasing. However, during plasma disruptions the positively biased electrode was sometimes much brighter than the rest of the field of view, corresponding to a large (>30 Amp) transient current in this electrode. These situations were not included in the data in this paper.

The center electrodes (E2 and E3) were also viewed from a nearby window from downstream along the local B field direction. From this direction some additional light was visible at the surface of the electrodes during biasing, mainly at the positive electrode (??). An attempt was made to cross-correlate these fluctuations in the light emission from the electrode surfaces with the Langmuir probes, but only a small and spatially diffuse correlation was observed (??). Occasionally a very small (~ few mm) bright spot of light was observed on the surface of an electrode at the same time that a bright spot of light was observed in the GPI view downstream. This was most likely due to a small arc at the electrodes (described below). These small and rare events did not contribute significantly to the data in this paper.

After the end of each of two run years the run the electrodes were examined inside the vessel. There were no large arc tracks and there was no significant melting of the electrodes or probes. There were many very small localized arc tracks (< 1 mm) on the surfaces of the electrodes, similar to the arc tracks over the whole inside of the (stainless steel) vacuum vessel. There

was also a thin coating on the electrodes due to plasma re-deposition, boronization and lithium evaporation, which did not significantly affect the electrical conductivity of the electrodes or the insulation of the boron nitride holder.

d) The fifth probe (P2)

For the discharges described in this paper there was a fifth Langmuir probe signal recorded, which was usually probe #2 located on the other side of electrode E2 (see Fig. 2). This probe was at the same radius as the first probe in the radial array (#3a), but 4 cm in the poloidal direction. For the normal polarity of the electrodes (E2 negative and E3 positive), this fifth probe was 0.5 cm from the negative electrode and ~4.5 cm from the positive electrode. The fifth probe was biased at +50 Volts like the other probes.

For the same Ohmic shots used for Figs. 6, 11 and 12 for electrode voltages ±70 V and ±90 V, the fifth probe's electron saturation current showed no significant change with bias "on" (0.175±0.04 Amps) vs. "off" (0.174±0.05 Amps). This is consistent with the results of Fig. 9, i.e. that the negatively biased electrode had no effect on the adjacent probe (however, the positive bias often did not affect the r=0 cm probe either).

For the same shots, the relative fluctuation levels and autocorrelation times in the fifth probe were also unchanged by biasing and similar to the results for the probe at r=0 cm in Fig. 11. However, there was a significant change with biasing in the zero-time-delay cross-correlation coefficient

between the fifth probe and probe #3a; namely, 0.095±0.11 with biasing "on" vs. 0.38±0.12 with biasing "off". This suggests that the local poloidal correlation length of the turbulence was *decreased* by the negative biased electrode, or that the poloidal correlation length was decreased by the relatively distant positive electrode.

e) Floating potential variation with electrode

Figure 14(a) shows the floating potential changes at a probe adjacent to a positively biased electrode. Here the floating potential on probe #P4 is plotted against the voltage on electrode #E3 for four shots in which electrode on the other side of this probe (i.e. #E4) was grounded. This data was for four Ohmic plasmas with I=0.8 MA and B=4.5 T(#124679-688), similar to those used for Fig. 6 and Fig. 7(c). Each point represents the average value in one "bias on" or "bias off" period. The floating potential on #P4 typically increases by +5-10 volts at for an E3 electrode voltage of +20-50 Volts. Thus the floating potential on the probe next to a positively biased electrode changes by ~10-20% of that electrode voltage.

Figure 14(b) shows the floating potential changes at a probe adjacent to a negatively biased electrode. Here the "O's" are the floating potential on probe #P2 vs. the voltage on electrode #E2 for shots in which electrode on the other side of this probe (i.e. #E1) was grounded, and the "x's" are the floating potential on probe #P2 vs. the negative voltage in the adjacent electrode #E1, for shots in which the electrode on the other side of this probe (#E2) was grounded. In both cases the floating potential on a probe next to a

negatively biased electrode does not change. This is consistent with the absence of SOL changes for a negatively biased electrode (Fig. 9).

There is considerable scatter in the floating potential response to the positive bias as shown in Fig. 14(a). This was most likely due to the variation in the outer gap and/or local SOL density over these shots and times. There was no clear correlation between these floating potential changes and the current drawn by electrode E3 in these cases.

f) Effect of GPI gas manifold

In this experiment the electrodes and the GPI diagnostic were intentionally aligned along a field line to try to measure the downstream effects of the biasing. However, this sometimes put the GPI gas manifold (which can be seen in Fig. 1) on B field lines which were connected to the electrodes, depending on the details of the plasma equilibrium. The GPI gas manifold was a stainless steel tube grounded to the vessel, so in principle this grounding could affect the flow of current and the potential in the electrode flux tube.

Figure 15 shows a check of this effect made by comparing two cases for five ±90 Volt biasing shots like that in Fig. 3: (a) near the end of the current ramp-up phase (≤0.11-0.15 sec) when all the field lines from electrode E3 were at least 1 cm radially inside and 1 cm radially below the manifold, and (b) during the steady current phase (0.2-0.3 sec) when about half of the field lines from electrode E3 were intersecting the manifold

(according to the equilibrium code EFIT). The result is that the effect of biasing is at least qualitatively the same with or without field line contact with the gas manifold. The differences between these two cases are on the same scale as the variations seen in other cases (Fig. 7), and so may be due in part to difference in the plasma density and/or outer gap in this region.

6. Comparisons with Theoretical Models

Section 6(a) compares the experimental results with the theory of divertor plate biasing, while Sec. 6(b) compares the results with other theories for the parallel and perpendicular penetration lengths of the bias potential. Section 6(c) describes a simple model for the relationship between these scale lengths and the expected SOL modification, and Sec. 6(d) describes a qualitative interpretation of the experimental results in terms of this simple model.

a) Comparison with theory divertor plate biasing

This experiment was motivated by the theories of Cohen, Ryutov et al on convective cell generation by divertor plate biasing [5-7]. Some of this theory is relevant to the present experiments at the outer midplane, whereas the divertor physics issues are not relevant.

The initial paper [5] proposed creating convective cells with divertor plate biasing. The condition for convective cell formation was that the

plasma potential change due to biasing was larger than the unperturbed radial potential variation across the cell. This appears to be the case in these experiments, since the floating potential change due to biasing, as shown in Fig. 7(c) and Fig. 14, was larger than the unbiased potential gradient, as shown in Fig. 7(c), at least over r=0 to 2 cm for the OH and NBI cases. This paper also compares the expected convective cell radial transport to Bohm diffusion. However, the far-SOL transport in NSTX is likely dominated by turbulent 'blobs' with a typical radial speed of ~1 km/sec [28]. For this experiment, the bias-induced convective cell transport would be larger than this blob transport for $E_{pol} > 2.5$ Volts/cm, which seems to be the case, assuming the measured potential changes occur over ~2 cm poloidally. A final point in this paper is that the parallel voltage drop due to the plasma resistance could 'consume' the bias potential if T_e was too low. However, for the present experiment with T_e ~8 eV (Fig. 5(a)) and $j_{||}$ ~10 A/10 cm^2 (for positive biasing), the resistive voltage drop is only ≤ 1 V/100 cm, which is small compared to the applied voltages of ~50 V. Thus the present experiment seems (at least marginally) to be within the regime of convective cell dominated transport, based on this model.

A second paper [6] discussed in more detail the sheath physics for biased plates. Assuming a model in which the electrode current flows along a magnetic flux tube of constant area to a grounded plate far downstream, it was shown that for *negative* biasing the plasma potential in this tube would not exceed ~$0.8T_e/e$, whereas for *positive* biasing the plasma potential would increase by ~$T_e/e \ln[\{\exp(e\varphi_b/T_e)+1\}/2]$, where φ_b is the plate bias potential. For the present experiment where T_e~10 eV and $e\varphi_b/T_e$~10, this implies that the plasma potential should change by about -8 Volts with negative bias and

by +90 Volts with positive bias. This asymmetry is at least qualitatively consistent with the asymmetrical SOL modification results of Fig. 9, although the measured potential changes are significantly smaller than these. The large ratio of positive to negative electrode current (~8) of Fig. 4(a) shows that there is significant cross-field current in this experiment. This is modeled in this paper by an effective area for collection at the downstream electrode, which for A=8 decreases the expected negative plasma potential to ~80 Volts, i.e. not significantly.

A third paper in this series [7] further discussed symmetry of positive vs. negative biasing through a model of divertor plate biasing which allowed cross-field currents near the X-point. Although this geometry is not relevant to the present experiment, the generic effect of a cross-field currents is to reduce the potential changes for the positive bias to the same level of those for negative bias. In the present experiment the electrode (I,V) characteristic (Fig. 4(a)) implies that there are cross-field currents, but their effect is not large enough to make the response symmetric (Fig. 9).

These papers also discuss the possibility of turbulence generation due to the shear flow in bias-induced convective cells is discussed; however, in the present experiment the turbulence level was already high without biasing, and *decreased* slightly with biasing (see Fig. 11(a)), so it is unlikely that the biasing created additional turbulence. This paper also calculated the heat load on the plates due to biasing, which in the present experiment is only ~10 Amps x 100 Volts ~1 kW, i.e. not significant in the SOL power balance.

b) Penetration lengths of the bias potential

The parallel and perpendicular scale lengths for the penetration of a biased electrode potential into a SOL plasma was discussed by Rozhansky [29] and Carlson [30]. The parallel penetration length was estimated to be $L_{||} \sim \lambda_{e,coll}(M_i/m_e)^{1/2}$, which is about the same as the parallel resistive scale length λ_{Spitz} [30], i.e. ~3-5x10^3 cm (see Table 1). This appears to be inconsistent with the absence of a clear perturbation due to electrode biasing at the GPI diagnostic ~100 cm along B, as discussed in Sec. 5(b).

Table 1: Theory for bias penetration scale lengths

$n = 10^{12}$ cm^{-3}

$T_e = 8$ eV

$n_o = 10^{12}$ cm^{-3} (assumed)

$\lambda_D \sim 10^{-3}$ cm

$\lambda_{e,coll} \sim 60$ cm

$L_{Spit} \sim 5x10^3$ cm

$L_{||} \sim 3x10^3$ cm

$R_{visc} \sim 1.1$ cm

$R_{inert} \sim 1.6$ cm

$R_{neut} \sim 0.8$ cm

The perpendicular penetration lengths for the electrode potential was evaluated in [29] assuming either viscous, inertial, or ion-neutral frictional forces. For this experiment these lengths are all ~1 cm, as shown in Table 1.

For these evaluations, the viscosity was taken to be anomalous (Bohm level), and the radial flow speed was taken to be the typical 'blob' speed of 1 km/sec, and a neutral density of $n_o \sim 10^{12}$ cm^{-3} was assumed based on recent measurements in NSTX [31].

These perpendicular scales are comparable to the radial potential scale length of ~1-2 cm seen in Fig. 7(c), and with a relatively small potential change at the probe ~0.5 cm from the electrode in the poloidal direction shown in Fig. 14(a). However, these perpendicular lengths were calculated assuming the large parallel scale lengths of the theory, which appears to disagree with the GPI data. Also, the Rozhansky model assumed that the electrode bias did not significantly perturb the density along the field line, and that the probe current is significantly below electron saturation, neither of which is the case in this experiment.

If, indeed, the parallel penetration length of the potential in this experiment was <100 cm, this suggest that the cross-field currents were much larger than those estimated above. There is presently no clear experimental indication of the cause for such currents. For example, there was no significant change in the electrode biasing response correlated with the GPI gas puff, which increased the local neutral density significantly. Although in previous electrode biasing experiments the neutral friction was considered to be an important mechanism for the radial current [8,9], for this experiment the estimated ion-neutral $\sigma_\perp \sim 10^{-3}$ $(\Omega\text{-m})^{-1}$ implies a negligible cross-field current of < 1 Amp over ~100 cm of the electrode flux tube.

c) Relationship of ExB flow to SOL profile modification

The theory discussed in Secs. 6(a)-(b) does not describe how the radial profiles of SOL density should be affected by the electrode biasing. This section describes a simple heuristic model which relates these ExB flows to the expected SOL density profile modifications.

Assume for the moment the simplified biasing geometry of Fig. 15(a). The magnetic field B is in the direction out of the paper, the electrode is in the radial vs. poloidal plane perpendicular B, and the density gradient (without bias) is in the radial direction. The electrode bias creates a perpendicular electric field $E_\perp$ at a distance $L_\perp$ from the center of the electrode, and this electric field extends in one direction along B by a distance $L_{||}$. The plasma within this convective cell also flows along B with a parallel speed $v_{||}$, and drifts across B with a perpendicular speed $v_\perp = E_\perp x B_z$ over $L_{||}$.

Assuming for the moment that this drift is the only mechanism for plasma transport across B, the number of plasma rotations N around B over a parallel transit time along the convective cell ($L_{||}/v_{||}$) is then:

$$N = v_\perp (L_{||}/v_{||})/(2\pi L_\perp) \qquad (1)$$

Thus N will depend upon the parallel and perpendicular penetration lengths, as well as the parallel and perpendicular velocities. For example, if $L_{||} \sim 50$ cm (half the distance to the GPI), $L_\perp \sim 3$ cm (based on Fig. 7(c)), $v_{||} \sim 10^6$

cm/sec (corresponding to a parallel Mach speed of $M_{||} \sim 0.5$ at 8 eV), and $v_{\perp} \sim 4x10^5$ cm/sec (corresponding to $E_{\perp}$= 10 V/cm at B=2.5 kG), then N ~ 1.

A simple model result for the *qualitative* effect of various rotations N on the local density profile is shown in Figs. 15(b). This model assumes a rigid-body rotation of the plasma in the $E_{\perp}$xB direction, along with some spread in $v_{||}$ to simulate a parallel thermal ion distribution. The initial density profile (N=0 case) is assumed to be linear over ±8 radial units (±4 units on either side the rotation axis) and constant in the poloidal and z directions. This initial density profile is rotated around the origin of Fig. 15(a) as follows: each successive step is the sum of ½ the density profile of the previous step rotated by 22.5º, plus ¼ of the previous step rotated by 45º, plus ¼ of the previous step but rotated by 0º. The radial profiles in Fig. 14(b) are plotted for a poloidal location 2 units below the rotation axis, in the direction corresponding to "outward" ExB flow.

The results of Fig. 15(b) are roughly as follows: a rotation of N=0.25 flattens the radial profile and raises its level, because this was previously the poloidal distribution at r = -2 units; a rotation of N=0.5 inverts the radial distribution, since this was previously the distribution along the negative radial direction; a rotation of N=0.75 flattens the radial profile and lowers its level, because this was previously the poloidal distribution at r = +2 units, and a rotation of N=1 brings back the distribution of N=0, except for a radial flattening due to the assumed spread in parallel rotation speeds. For large N>>1, the radial distribution becomes flat at a level of 0.5 due to this spreading.

d) Qualitative interpretation of the radial profiles

This qualitative model can be used to interpret some of the experimental results of Sec. 4 by considering the expected ExB flow patterns as shown in Fig. 16. This figure shows electrodes E2 and E3 along with the radial probe array, with the radially outward direction to the right. The dark circles show the expected flow due to the positively biased electrode, which is assumed to be dominant, and the light circles show the expected flow due to the negatively biased electrode, which has almost no effect (Fig. 9).

For the "normal" biasing case of Fig. 16(a), the radial ExB flow is outward at the probe array, and so the model results of Fig. 13(b) can be compared to the experimental profiles of Fig. 6(a). The measured profiles first flatten up about ±50 Volts, and then partially reverse at up to ±90 Volts. The closest qualitative fit to the model seems to N ~ 0.25 at ±50 Volts and N ~ 0.5-0.75 at ± 90 Volts. Of course this fit is not very good in detail, since the model does not use the actual radial profile for N=0, which was not even known for radii r < 0 cm. For other experimental cases, such as for NBI and OH in Fig. 7(a), the profiles flatten at a higher level similarly to the model case for N=0.25, but again the fit to the model is only qualitative.

The model results of Sec. 6(c) for a poloidal location 2 units above the rotation axis, i.e. for the direction corresponding to "inward" ExB flow, are the same as Fig. 15(b) except that the N=0.25 and N=0.75 labels are switched. This can be compared with the experimental results for the "reversed" polarity in Fig. 8(a), where the expected flow directions are indicated in Fig. 16(b). The closest qualitative fit to the model seems to be

at N ~ 0.5, but again this fit is not good in detail, and in particular does not explain the very low signal seen at r = 0 cm in the reversed bias case.

The result of Fig. 8(b) when *both* electrodes were positive could be qualitatively interpreted either in terms of one clockwise convective cell around each of the electrodes, or one large clockwise convective cell around both electrodes, as illustrated in Fig. 16(c). In the former case little or no change in the radial profile would be expected at the probes, since the ExB drifts from the two electrodes would approximately cancel. In the latter case, which would occur if the perpendicular penetration length of the potential was larger than the electrode spacing, a decrease in the flux to the probe at r=0 cm would be expected since the normal radial flow of plasma to this probe would be interrupted by this ExB flow. An increase in the flux to the outermost probe at r=3.75 cm might also be expected if this flow went around the electrodes as shown in Fig. 16(c). If so, the closest fit to the model would again be the N ~ 0.5 case of Fig. 15(b), although it is surprising that the profile should be so similar to the reversed case of Fig. 8(a).

In summary, there is some qualitative similarity of the measured profile changes during electrode biasing and a simple model based on an ExB convective cell rotation of N ~ 0.5 at ±90 Volts bias. However, there are many details which are yet not modeled correctly, e.g. the unbiased density profile inside the r=0 location, which was not measured. Possible improvements to this modeling are discussed in Sec. 7(c).

7. Summary and Discussion

a) Summary of experimental results

In this experiment a local poloidal electric field was created by a pair of biased electrodes in the SOL of NSTX. The main experimental results can be summarized as follows:

1) the particle flux and floating potential between the electrodes was strongly modified by the biased electrodes (Figs. 6-7),

2) the radial width of the SOL profile increased for an outward ExB drift, but inverts for an inward ExB drift, or for a ++ polarity (Fig. 8),

3) these changes are dominantly caused by the positively biased electrode, with almost no changes due to the negatively biased electrode (Figs. 9 and 14),

4) the local turbulence measured between these electrodes was only slightly perturbed by this biasing (Figs. 11-12),

5) the radial D_α profiles and turbulence measured ~100 cm downstream from the electrodes along B was not significantly changed by the biasing (Fig. 13).

b) Open issues on the comparisons with theory

The observed changes in the SOL width due to biasing were at least qualitatively consistent with the expected flows due to ExB drifts, as discussed in Sec. 6(b)–(d) . However, any quantitative modeling of these profile changes requires knowledge of several parameters which were not measured, e.g. the parallel and perpendicular penetration lengths of the bias potential, and the density profile inside the radius of the probe array. Thus there is at present no quantitative understanding of the profile results, e.g. for the variation with electrode voltage (Fig. 6) or the similarity between the results for reversed and ++ biasing shown in Fig. 8, or the relatively small effect with floating electrodes (Fig. 10).

The strong asymmetry observed between the effects of positive and negative biasing were predicted by the modeling of Cohen and Ryutov, as discussed in Sec. 6(a). This is due to the large expected voltage drop across the negative sheath. However, the relatively small potential change near the positive electrode (Fig. 14(a)) was not predicted by theory. Therefore either the potential drop across the negative sheath was a large fraction of the applied voltage, or the perpendicular scale of the potential perturbation with a positive electrode was significantly less than 0.5 cm.

The most direct measurement of the effect of biasing on the ExB drifts in this experiment was the radial propagation speed of the turbulence, which should have been increased by a locally outward E_{pol}xB drift velocity. There was a marginally significant ~1 km/sec increase in the measured radial turbulence velocity in the probe array with outward ExB biasing (Fig.

12(b)), but this was far smaller than the expected effect of the applied E_{pol}xB drift (e.g. ~20 km/sec at 50 V/cm). There was also a marginally significant ~0.4 km/sec increase in the radial turbulence velocity at the GPI location (Fig. 13(b)). Although these changes were small, they are not inconsistent with the relatively small number of convective cell rotations N~0.5 inferred from the model of Sec. 6(d). The relatively small magnitude of these E_{pol}xB drifts has not yet been explained by theory.

The large ratio of the electron to ion current drawn by the electrode, as shown in Fig. 4(a), indicates that there is a significant cross-field current in this experiment (as usual for probes or electrodes in tokamaks). The origin of this cross-field current is not understood. This anomalous cross-field current may have caused the relatively small response observed with the 'floating electrodes', as shown in Fig. 10, since the current path from positive to negative electrodes is shorter than from the positive electrode to vessel ground (normal polarity), which reduced the parallel penetration length of the potential.

Perhaps the most surprising result of this experiment was the small effect of the biasing on D_α profiles and turbulence seen in the GPI diagnostic ~100 cm downstream along B (Fig. 13), even though the turbulence was highly correlated over this distance. This is at first sight not consistent with the large parallel scale lengths for potential changes predicted by theory, as discussed in Sec. 6(b). However, this could be explained if the positive potential perturbation in the flux tube was much smaller than the applied potential, such that the v_{rad} due to this potential were less than the ambient turbulence speed.

The turbulence levels themselves were not increased by the electrode biasing, as considered in [6], but actually decreased (Fig. 11(a)). The effect of ExB shear flow on turbulence is important for this experiment and for SOL transport in general, but is not yet well understood [32 and references therein].

c) Directions for improvement

The next step for this experiment would be to install electrodes in the divertor plates to determine how well this type of biasing can control the SOL plasma near the divertor strike zone. Plans are underway install several electrodes on future divertor tiles in NSTX. For further experiments at the outer midplane, it would be useful to have a movable electrodes and a way to easily vary their size or shape.

On the diagnostic side, the biggest improvement would come from an increase in the number of probes around the electrodes. Ideally a 2D array of probes around the electrode could be used to map out the 2D potentials and flows due to the biasing. Downstream probes would also be valuable to understand the parallel propagation of the potential. Downstream magnetic sensors would also be useful to measure the currents caused by biasing (the magnetic sensors in NSTX were too far away from the electrode field lines to detect any perturbation in the present experiment).

On the theoretical side, the effects of intermittent SOL turbulence or 'blobs' could be incorporated into the modeling of this experiment, since the

electrode current has a large fluctuation level due to blobs (Fig. 3), and blob size is comparable to the electrode size (Fig. 12(a)). For example, the ExB flow induced by the electrode might be limited by the blob diameter, and the blob transit time across the electrode flux tube may be comparable to the convective cell rotation time. Another possibility effect is the finite ratio of ion gyroradius to electrode spacing (~0.2 cm/1 cm), which could cause some ion orbit transport over this spacing.

Acknowledgments: We thank J.A. Boedo, D. D'Ippolito, E.D. Fredrickson, H.E. Kugel, R. Maingi, B.D. Scott, and V. Soukhanovskii for discussions about this work, which was supported by U.S. DOE Contract # DE-AC02-76CH03073. This work performed under the auspices of the U.S. Department of Energy by Lawrence Livermore National Laboratory under Contract DE-AC52-07NA27344.

Figure Captions:

1. Photo of the outer wall of NSTX showing the location of the electrodes and probes in this experiment. The holder for the electrodes and probes was ~25º below the outer midplane, and oriented so that the plane of the electrodes was approximately normal to the total magnetic field during plasmas. The electrode mounting plate was ~ 1 cm radial behind the shadow of the RF antenna just behind it. The gas puff imaging (GPI) manifold was ~1 meter along B in the other direction.

2. Scale drawing of the electrodes and probes. The four 3 cm x 3 cm electrodes were flush mounted into a boron nitride holder and separated in the local poloidal direction with a gap of ~ 1 cm between them. The leading edges of the electrodes were ~ 0.3 cm behind the leading edge of the holder. There were 8 flush-mounted stainless steel Langmuir probes of 0.3 cm diameter in the electrode holder, four of them in a radial array between electrodes E2 and E3 (#P3a-P3d).

3. Typical time dependences of some plasma parameters along with electrode and probe signals (#129501). On the slower timescale in (a), the plasma current, outer gap, and line-averaged density are shown along with the electrode voltages, which were modulated at 50 Hz (at constant voltage). On a faster timescale in (b) are the electrode voltages and currents, and also a probe current (bottom trace). The high frequency fluctuations in the electrode and probe currents are due to SOL turbulence.

4. In (a) is the dependence of the electrode current on the electrode voltage. The "normal" curve is for the usual case where the electrodes are biased with respect to the (grounded) wall. Each point represents the current drawn by either the positively biased electrode E3 or the negatively biased electrode E2, averaged over 0.2-0.3 sec in similar shots. The "float" point was when the electrode E3 was biased with respect to E2. In (b) is the current vs. voltage for probe #P3a, both with "bias on" (E3 at +90 V and E2 at – 90 V) and "bias off". The probe points are each averaged over ~14 voltage sweeps (#129506).

5. Electron temperature and density profiles inferred from the probe sweeps such as those in Fig. 4(b). The horizontal scale is the radial position of the probes in the radial array measured with respect the first probe (#P3a), which is centered between electrode E2 and E3 (see Fig. 2). In (a) are the T_e profiles, which show a slight increase in temperature with biasing. In (b) are the ion saturation ("isat") and (near-)electron saturation ("esat") current profiles, with the density scale at left inferred from the ion saturation current profile. The 'esat' data are normalized to the 'isat" points at r=0. There is a similar change in the both the "isat" and "esat" profiles with this ±90 V biasing.

6. In (a) is the variation of the probe electron saturation current profiles as a function of applied electrode bias voltage for a set of Ohmic discharges. The biasing was applied to electrodes E2 and E3 with equal and opposite voltage, with the E_{pol}xB drift direction outward between them. In (b) is the ratio "bias on" to "bias off" current for many cycles for the 2.5 cm probe. The red line in (b) is a fit to the circled points, which are for the same cases

as for (a). There is a fairly large scatter in the results, but not much systemativ variation over this range of plasma conditions.

7. Other examples of electrode biasing effects on the radial profiles. In (a) are the electron saturation current profiles for "bias on" and "bias off" for Ohmic, RF, and NBI plasmas, and in (b) are the ratios of the "bias on" to "bias off" probe currents at r=2.5 cm. In (c) are floating potential profiles with "bias on" (solid lines) and "bias off" (dashed lines) for OH, NBI, and RF cases. The potentials increase with biasing by $\leq$ 10 V, which is much smaller than the bias voltage of ±50-90 V.

8. Part (a) shows the electron saturation current profiles when the electrode polarity was reversed, i.e. with E2 positive and E3 negative (at the same voltage), so that the E_{pol}xB drift was radially *inward* at the probe array. Part (b) shows the electron saturation current profiles when the electrode polarities of E2 and E3 were *both positive* (at the same voltage). The profiles with this biasing were similar to the reversed polarity case of (a), i.e. with the with current in the outermost probe ~10 times that of the innermost probe.

9. Part (a) shows the electron saturation current profiles when E3 was +50 V and E2 was grounded (along with E1 and E4), while (b) shows the case when electrode E2 was -50 V and E3 was grounded (along with E1 and E4). The effects of biasing with only one electrode at +50 V were similar to those with ±50 V biasing (not shown), while the effects of biasing with only one electrode at -50 V were negligible.

10. The effect on the electron saturation current profiles when electrode E3 was biased +90 V with respect to E2, i.e. the two electrodes E2 and E3 were floating with respect to ground (as in a double probe). The SOL profile is broadened, but considerably less than with the ±90 V biasing with respect to ground.

11. The effect of biasing on the relative probe current fluctuation levels and autocorrelation times for a set of Ohmic discharges with normal biasing (radial ExB drift outward). The relative fluctuation levels show a systematic decrease by up to x2 in the radial regions where the local density was increased with biasing (as in Fig. 5). The autocorrelation times are slightly, but not significantly, decreased by the biasing.

12. The effect of biasing on the cross-correlations between the probe at r=0 cm and the other probes in the radial array. The biasing has no effect on the radial cross-correlation coefficients. There was an small increase in the outward radial propagation speed with biasing from ~1.4 km/sec to ~2.3 km/sec, but this increase was only slightly outside uncertainty these measurements.

13. Part (a) shows the radial profile of the average D_α light seen by the GPI diagnostic at the same poloidal location as the probe array over -6 cm to +2 cm with respect to the r=0 cm probe location. There was no measurable perturbation due to the electrode biasing in this D_α profile. Part (b) shows the delay times of the peak of the cross-correlation function vs. radius for the turbulence propagation, as for Fig. 12(b). There was a slight increase in the

outward radial propagation speed with biasing, but only slightly outside the measurement uncertainty.

14. Part (a) shows the floating potential measured on probe #P4 as a function of the positive voltage in the adjacent electrode #E3 when electrode on the other side of this probe (#E4) was grounded. The floating potential on the probe next to this positively biased electrode changes by ~10-20% of the applied electrode voltage. Part (b) shows the floating potential measured on probe #P2 as a function of the negative voltage in the adjacent electrode #E3 or #E1 when the electrode on the other side of this probe was grounded. In these cases the floating potential on a probe next to a negatively biased electrode does not change significantly.

15. Effect of the gas manifold field line connection on the radial profile of the probe electron saturation current profiles with and without biasing. The biasing was applied to electrodes E2 and E3 with the E_{pol}xB drift direction outward between, as in Fig. 6. Case (a) was when the field lines from electrode E3 were not connected to the gas manifold, and case (b) was when the field from electrode E3 were partially connected to the manifold. The effect of biasing is at least qualitatively similar between these two cases.

16. Part (a) shows the geometry for a qualitative model for the effect of biasing on the SOL profiles. The magnetic field B is in the direction out of the paper, the electrode is in the radial vs. poloidal plane perpendicular B, and the density gradient (without bias) is in the radial direction. Part (b) shows the profiles for various convective cell rotations N for an initial profile (N=0). These profiles are plotted for a poloidal location 2 units

below the rotation axis, in the direction corresponding to outward E_{pol}xB flow.

17. Qualitative picture of the expected ExB flow patterns for various biasing configurations of electrodes E2 and E3 (squares), along with the radial probe array (dots), with the radially outward direction to the right. Case (a) is for normal polarity (outward E_{pol}xB flow between the electrodes), case (b) is for reversed polarity, and case (c) is for both electrodes positive. The dark circles show the expected flow due to the positively biased electrode, which is presumed to be dominant, and the light circles show the expected flow due to the negatively biased electrode, which had almost no effect (Fig. 9).

References

[1] B. Lipschultz et al, Nucl. Fusion **47**, 1189 (2007)

[2] A. Loarte, Nucl Fusion **47** S203 (2007)]

[3] P. Staib, J. Nucl. Mat. **111/112**, 109 (1982)

[4] W. Fundamenksi, Fusion Science and Technology **53**, 1023 (2008).

[5] R.H. Cohen and D.D. Ryutov, Nucl. Fusion **37**, 621 (1997),

[6] D.D. Ryutov et al, Plasma Phys. Cont. Fusion **43**, 1399 (2001),

[7] R.H. Cohen et al, Plasmas Phys. Cont. Fusion **49**, 1 (2007)

[8] van Oost, G. et al, Plasma Phys. Cont. Fusion **54**, 621 (2003)

[9] R. R. Weynants et al, Fus. Science and Tech. **47** (2005)

[10] E. Strait, Nucl. Fusion **21**, 943 (1981)

[11] R. Decoste et al, Phys. Plasmas **1**, 1497 (1994)

[12] M.J. Schaffer et al, Nucl. Fusion **36**, 495 (1996)

[13] R.P. Doerner et al, Nucl. Fusion **34**, 975 (1994)

[14] R.W. Motley and J. Glanz, Phys. Fluids **25**, 2107 (1982)

[15] B. LaBombard, Nucl. Fusion **30**, 485 (1990)

[16] R.A. Pitts and P.C. Stangeby, Plasma Phys. Cont. Fus. **32**, 1237 (1990)

[17] D.L. Winslow et al, Phys. Plasmas **5**, 752 (1998)

[18] H. Thomsenet al, Plasma Phys. Cont. Fusion **47**, 1401 (2005)

[19] D.L. Winslow and B. LaBombard, J. Nucl. Mat. **290-293**, 788 (2001)

[20] V.A. Rozhanski, et al, Nucl. Fusion **39**, 613 (1999)

[21] A. Carlson, Phys. Plasmas **8**, 4732 (2001)

[22] J. Hara et al, J. Nucl. Mat. **241-243**, 338 (1997)

[23] G. Counsell et al, J. Nucl. Mat. **313-316**, 804 (2003)

[24] J. Stockel et al, Plasma Phys. Cont. Fusion **47**, 635 (2005)

[25] A.L. Roquemore et al, Rev. Sci. Inst. **79**, 10F124 (2008),

[26] S.J. Zweben et al, J. Nucl. Mat. … (2009)

[27] S.J. Zweben et al, Phys. Plasmas **13**, 056114 (2006)

[28] S.J. Zweben et al, Nucl. Fusion **44** (2004) 134

[29] V.A. Rozhansky et al, Nucl. Fusion **39**, 613 (1999);

[30] A. Carlson, Phys. Plasmas **8**, 4732 (2001)

[31] P.W. Ross, Private communication (2009)

[32] T.A. Carter and J.E. Maggs, Phys. Plasmas **16**, 012305 (2009)

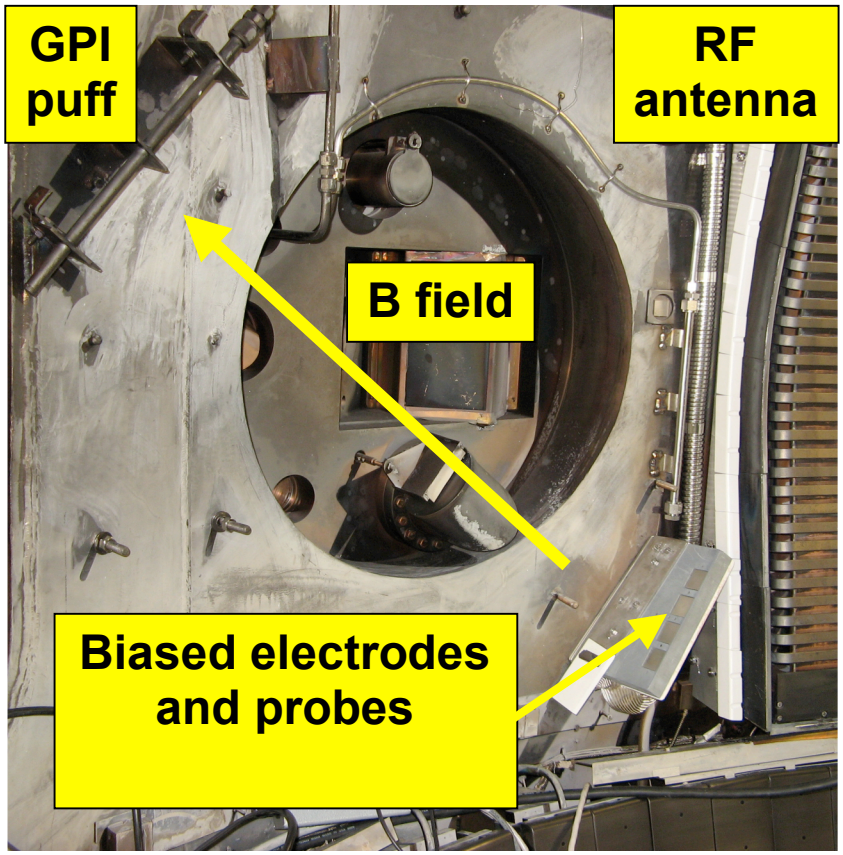

Fig. 1

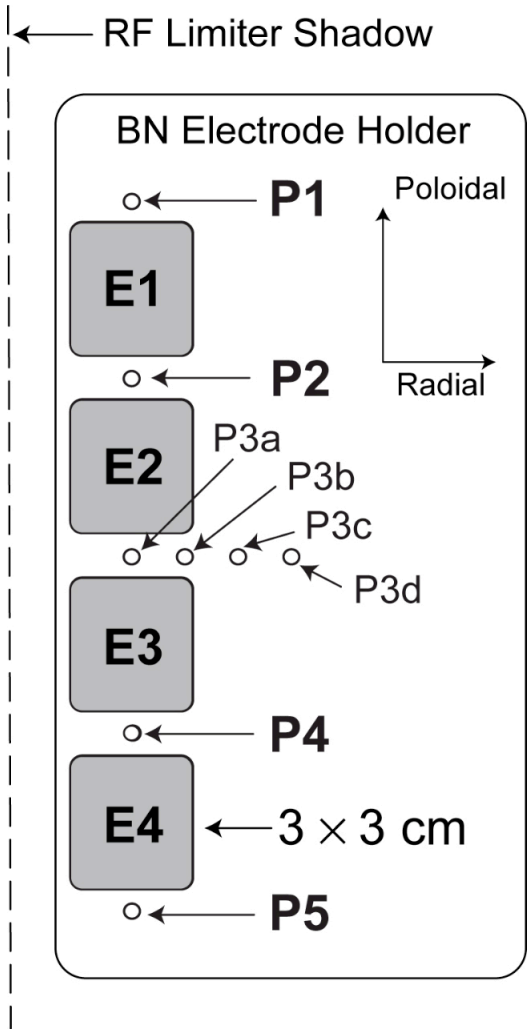
RF Limiter Shadow
BN Electrode Holder
P1
Poloidal
E1
P2
Radial
E2
P3a
P3b
P3c
P3d
E3
P4
E4
3 × 3 cm
P5

Fig. 2

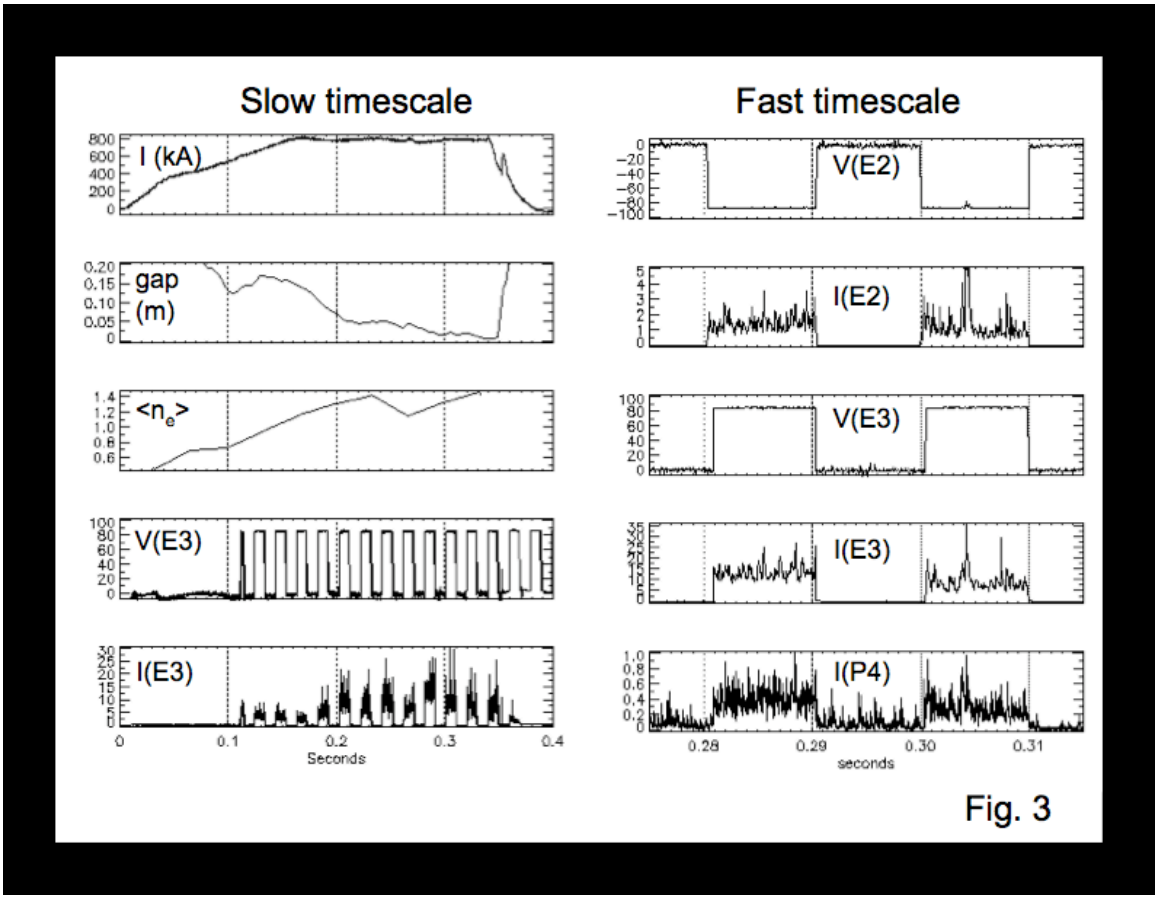
Slow timescale
Fast timescale
I (kA)
gap (m)
<n_e>
V(E3)
I(E3)
V(E2)
I(E2)
V(E3)
I(E3)
I(P4)
Seconds
seconds

Fig. 3

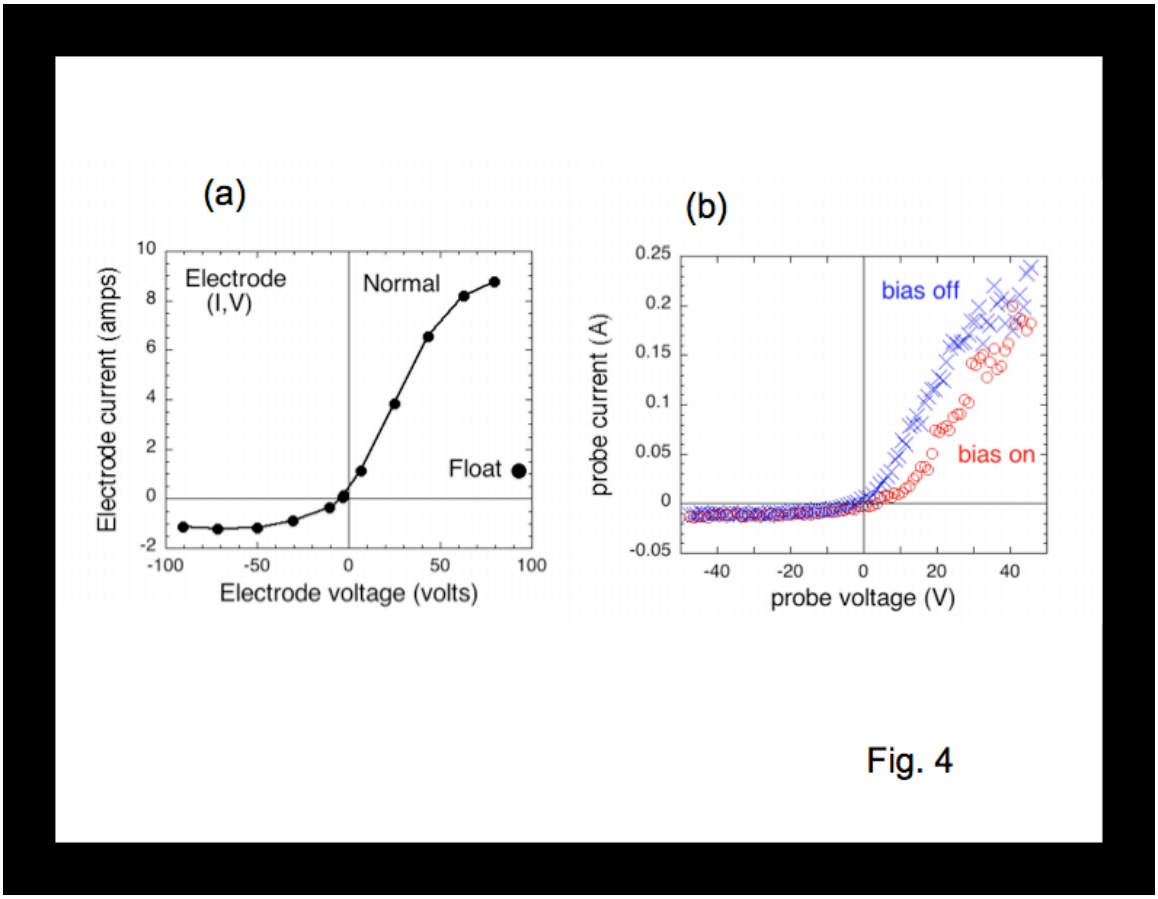
(a)
Electrode
(I,V)
Normal
Float
Electrode current (amps)
Electrode voltage (volts)
10
8
6
4
2
0
-2
-100
-50
0
50
100
(b)
bias off
bias on
probe current (A)
probe voltage (V)
0.25
0.2
0.15
0.1
0.05
0
-0.05
-40
-20
0
20
40

Fig. 4

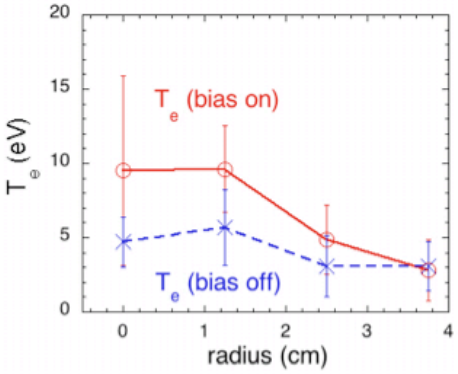
20
15
10
5
0
T_e (eV)
T_e (bias on)
T_e (bias off)
0
1
2
3
4
radius (cm)

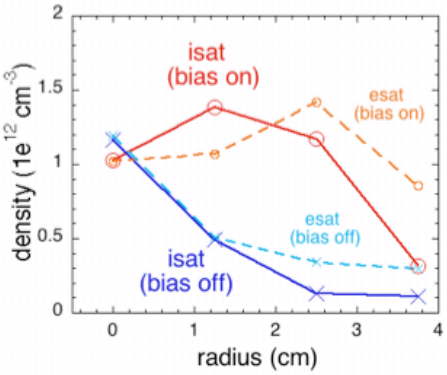
2
1.5
1
0.5
0
density (1e^12 cm^-3)
isat
(bias on)
esat
(bias on)
esat
(bias off)
isat
(bias off)
0
1
2
3
4
radius (cm)

Fig. 5

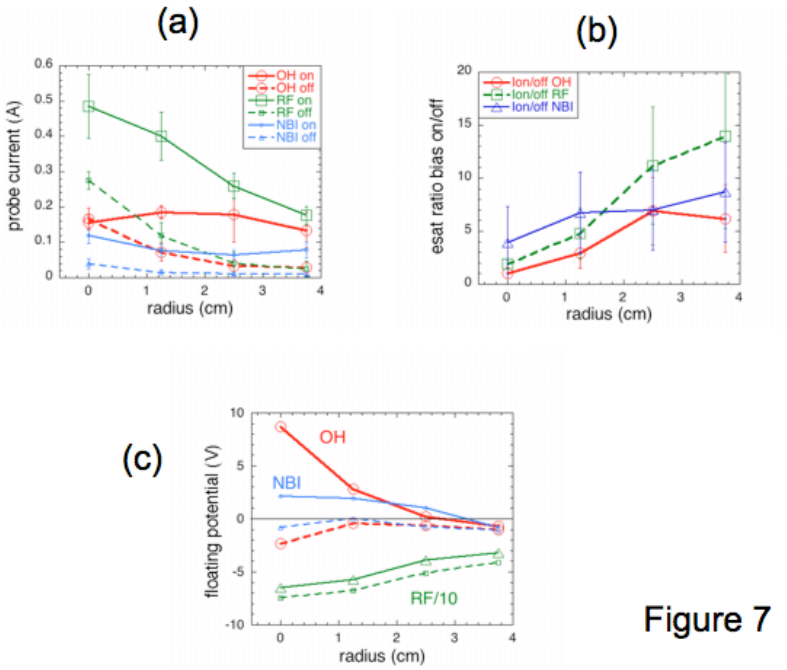
(a)
probe current (A)
radius (cm)
OH on
OH off
RF on
RF off
NBI on
NBI off
(b)
esat ratio bias on/off
radius (cm)
Ion/off OH
Ion/off RF
Ion/off NBI
(c)
floating potential (V)
radius (cm)
OH
NBI
RF/10

Figure 7

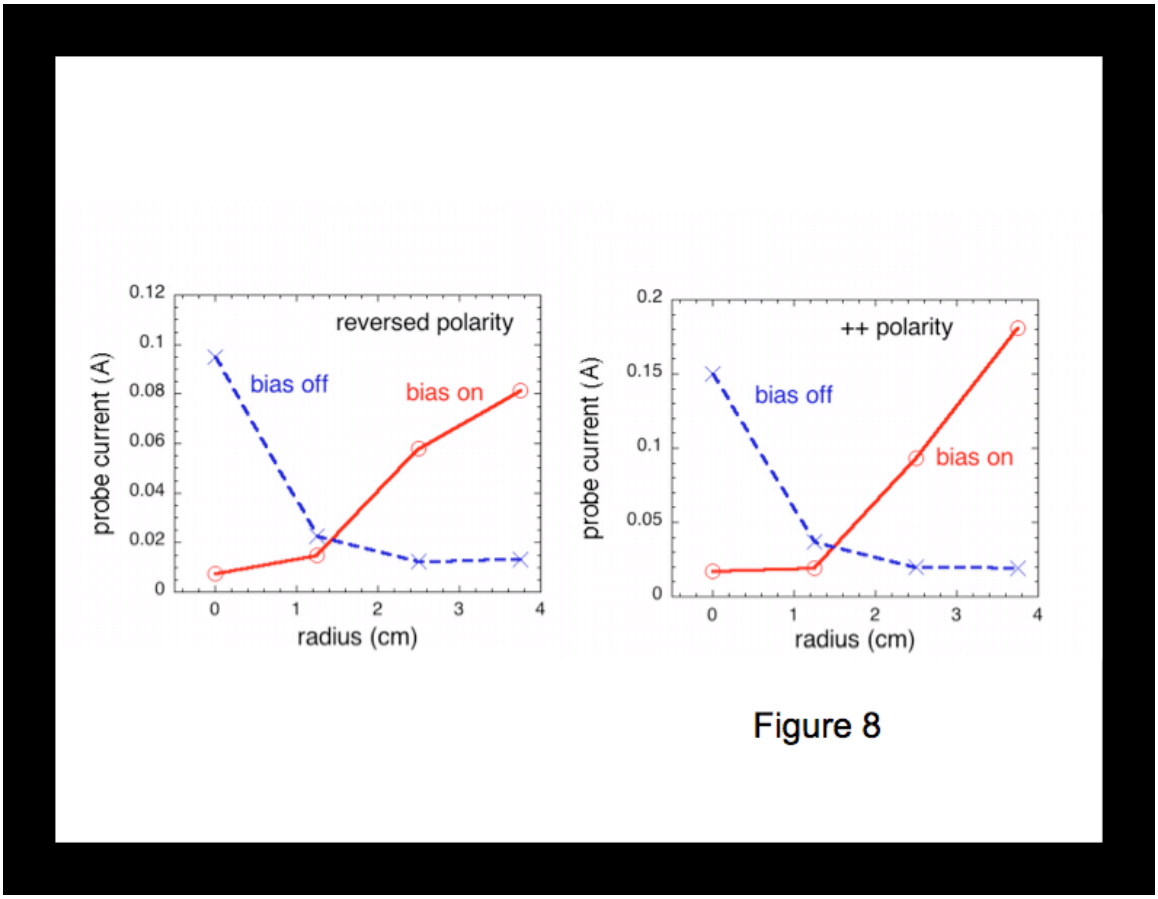
reversed polarity
bias off
bias on
probe current (A)
radius (cm)
0.12
0.1
0.08
0.06
0.04
0.02
0
0
1
2
3
4
++ polarity
bias off
bias on
probe current (A)
radius (cm)
0.2
0.15
0.1
0.05
0
0
1
2
3
4

Figure 8

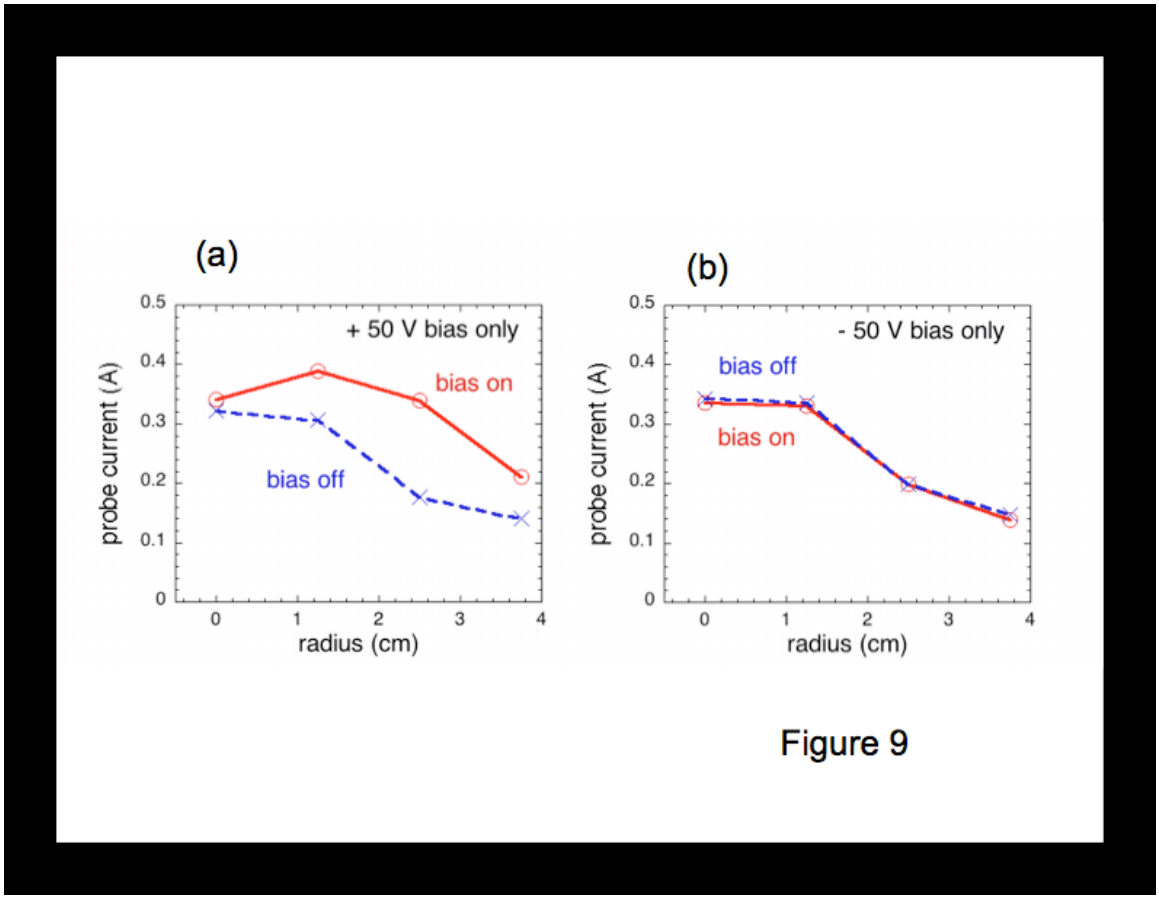
(a)
+ 50 V bias only
bias on
bias off
probe current (A)
radius (cm)
(b)
- 50 V bias only
bias off
bias on
probe current (A)
radius (cm)

Figure 9

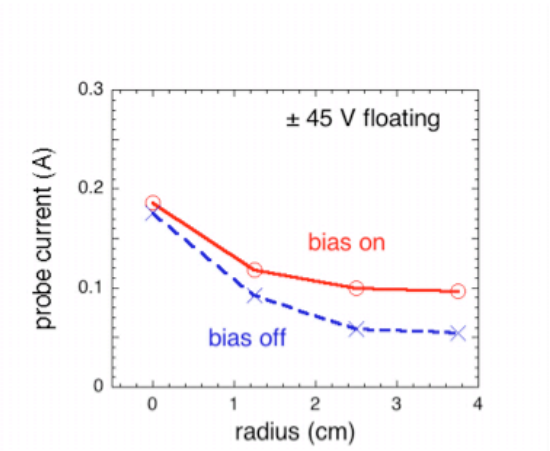
± 45 V floating
bias on
bias off
probe current (A)
radius (cm)
0.3
0.2
0.1
0
0
1
2
3
4

Figure 10

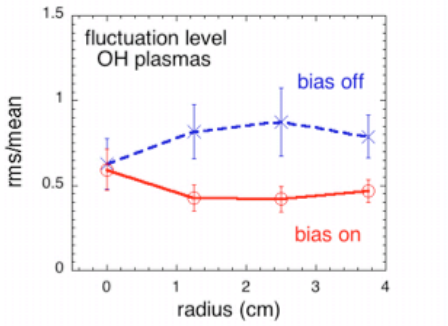
fluctuation level
OH plasmas
bias off
bias on
rms/mean
radius (cm)
1.5
1
0.5
0
0
1
2
3
4

(a)

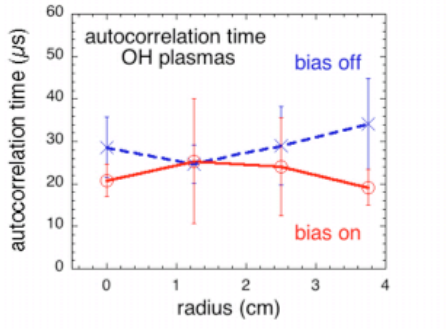
autocorrelation time
OH plasmas
bias off
bias on
autocorrelation time (μs)
radius (cm)
60
50
40
30
20
10
0
0
1
2
3
4

(b)

Figure 11

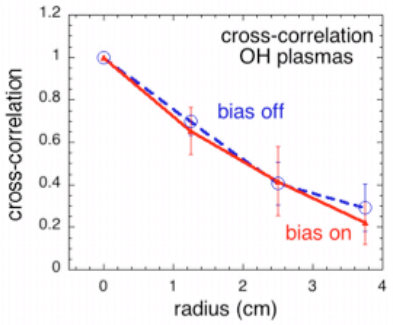
cross-correlation
OH plasmas
bias off
bias on
cross-correlation
radius (cm)
1.2
1
0.8
0.6
0.4
0.2
0
0
1
2
3
4

(a)

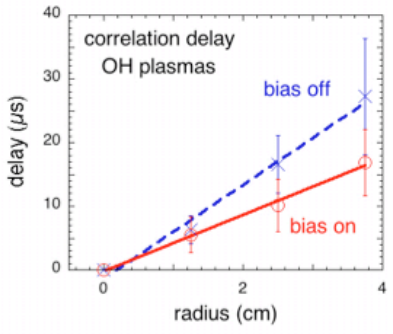
correlation delay
OH plasmas
bias off
bias on
delay (μs)
radius (cm)
40
30
20
10
0
0
2
4

(b)

Figure 12

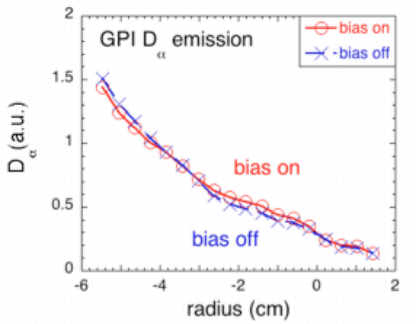
GPI D α emission
bias on
bias off
D α (a.u.)
radius (cm)
(a)
GPI correlation delay
bias on
bias off
origin
delay (μs)
radius (cm)
(b)

Figure 13

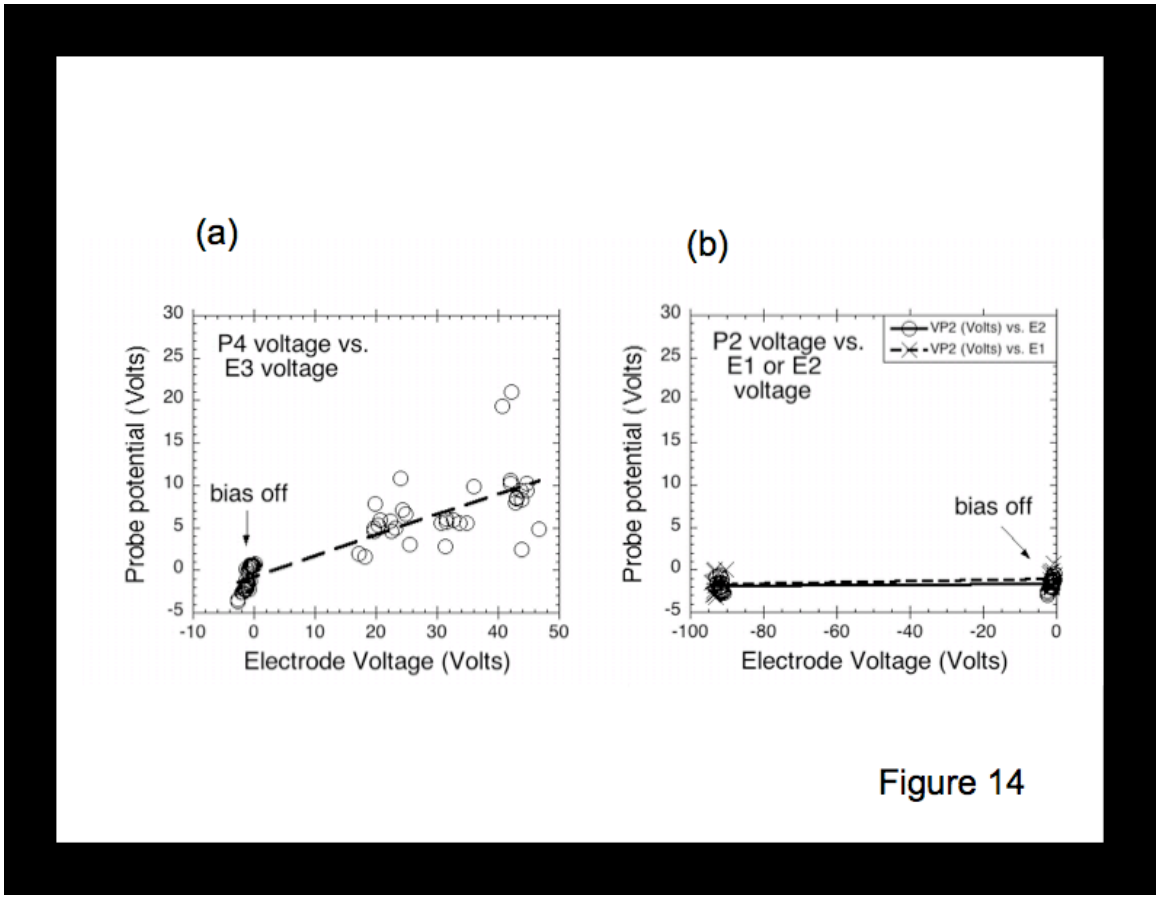
(a)
P4 voltage vs.
E3 voltage
bias off
Probe potential (Volts)
Electrode Voltage (Volts)
(b)
P2 voltage vs.
E1 or E2
voltage
VP2 (Volts) vs. E2
VP2 (Volts) vs. E1
bias off
Probe potential (Volts)
Electrode Voltage (Volts)

Figure 14

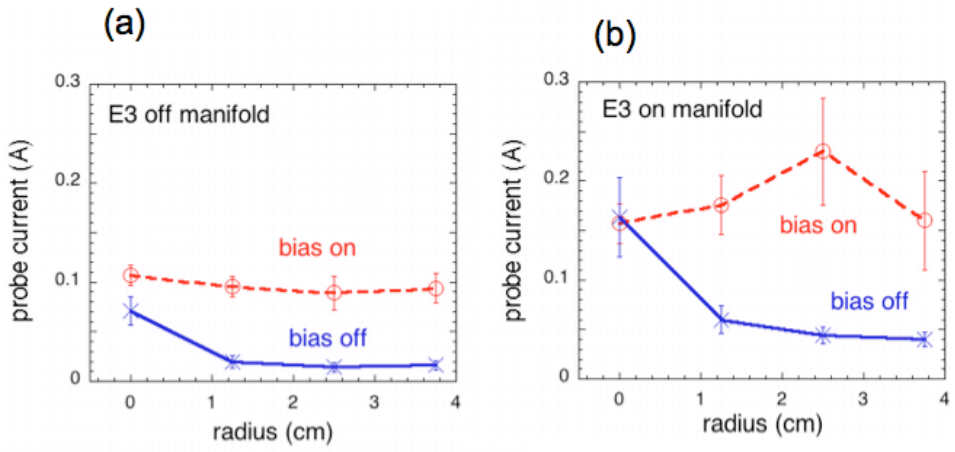
(a)
E3 off manifold
probe current (A)
0.3
0.2
0.1
0
bias on
bias off
0
1
2
3
4
radius (cm)
(b)
E3 on manifold
probe current (A)
0.3
0.2
0.1
0
bias on
bias off
0
1
2
3
4
radius (cm)

Figure 15

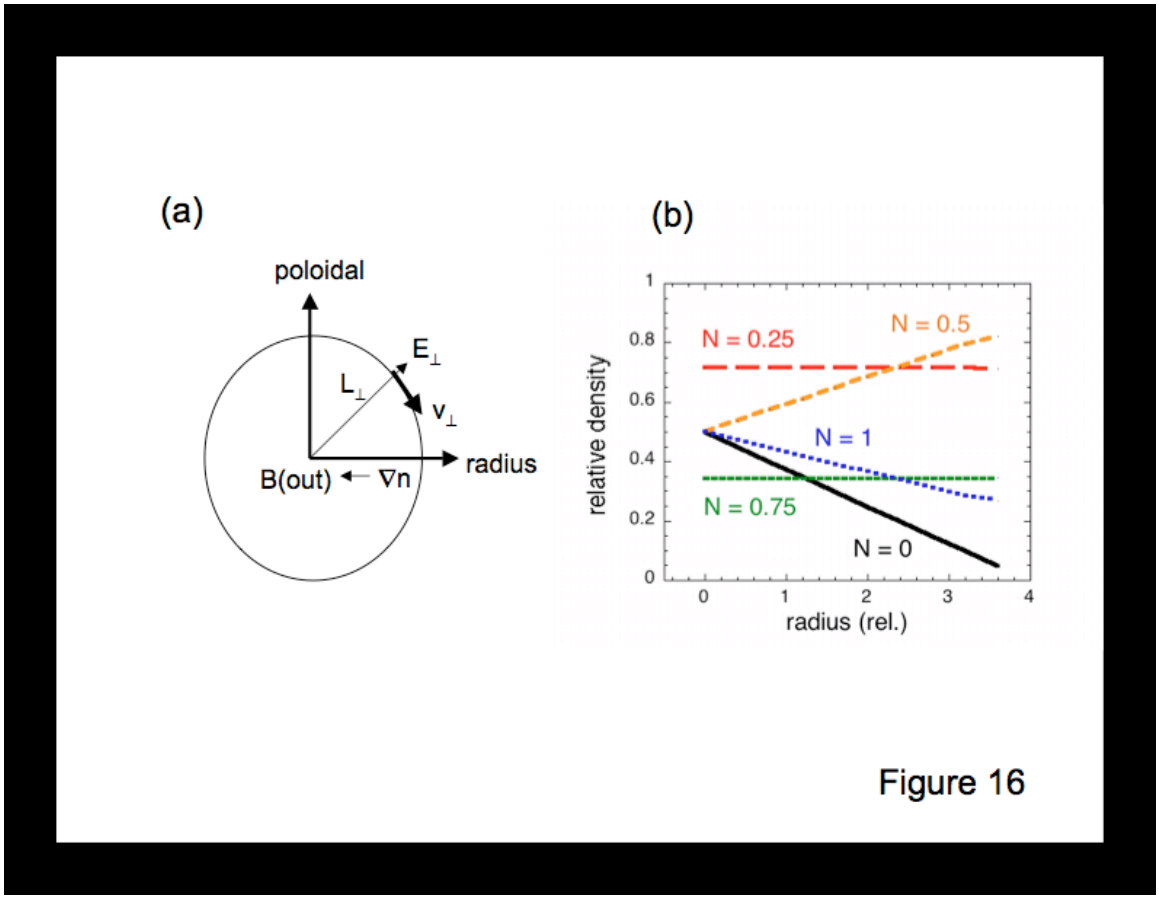
(a)
poloidal
E⊥
L⊥
v⊥
B(out)
∇n
radius
(b)
relative density
radius (rel.)
N = 0.25
N = 0.5
N = 1
N = 0.75
N = 0
0
0.2
0.4
0.6
0.8
1
0
1
2
3
4

Figure 16

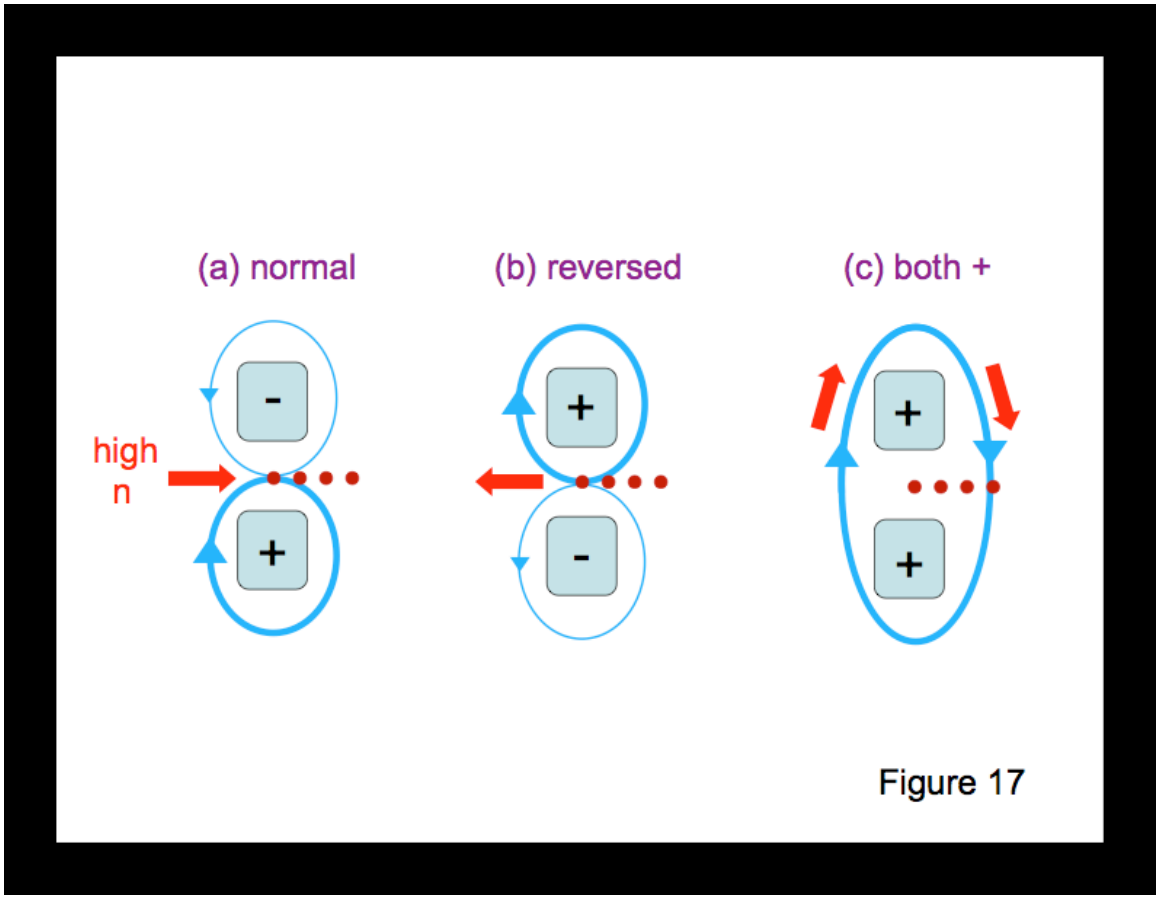

Figure 17